Ionization-induced thermally activated defect-annealing process in SiC

Aurélien Debelle,[1] Lionel Thomé,[1] Isabelle Monnet,[2] Frédérico Garrido,[1] Olli H. Pakarinen,[3] and William J. Weber[3,4]
[1]*Centre de Sciences Nucléaires et de Sciences de la Matière (CSNSM), Université Paris-Sud, CNRS/IN2P3, Université Paris-Saclay, 91405 Orsay, France*
[2]*CIMAP, Normandie Université, ENSICAEN, UNICAEN, CEA, CNRS, 14000 Caen, France*
[3]*Materials Science and Technology Division, Oak Ridge National Laboratory, Oak Ridge, Tennessee 37831, USA*
[4]*Department of Materials Science and Engineering, University of Tennessee, Knoxville, Tennessee 37996, USA*

(Received 24 April 2019; published 20 June 2019)

Ionizing events can lead to panoply of irradiation effects, and in silicon carbide (SiC), they drastically modify the defect production rate or the initial density. To better understand this phenomenon, 6H-SiC single crystals were first predamaged using low-velocity 100-keV Fe^+ ions at three fluences in the range of $10^{14}\,cm^{-2}$ to induce three different initial disorder levels peaking at values between ∼0.8 and 1 (1 corresponding to full amorphization). Crystals were then submitted to swift heavy ion irradiation in the $10^{13}\,cm^{-2}$ fluence range at both low (∼100 K) and high (∼770 K) temperature. Rutherford backscattering spectrometry in channeling conditions revealed that swift ions allow annealing part of the initial damage, the recovery efficiency increasing with the irradiation temperature and reaching 75% in initially severely disordered crystals. This temperature effect has been qualitatively predicted by molecular dynamics simulations. Transmission electron microscopy allowed imaging both the recovery and the difference in the microstructure of the layers irradiated at low or high temperature. Recovery cross sections are found to lie in the range of a few square nanometers, consistent with previously reported values. A scenario for a general, two-step annealing mechanism referred to as an ionization-activated, thermally assisted defect-annealing (IATADA) process is proposed. This mechanism rationalizes the diverse descriptions reported so far in the literature.

DOI: 10.1103/PhysRevMaterials.3.063609

I. INTRODUCTION

Ion/solid interactions applied to materials science represent a vast, active research field [1,2] in which some questions remain to be elucidated. One typical example is the actual effect of energy deposition on the atomic network of materials. Indeed, energy transfer from the energetic particles to the target electrons and/or nuclei can lead to a panoply of responses, depending on both the projectile characteristics (mainly nature and energy) and the material physical properties (which are mostly governed by the electronic structure). Understanding the effect of energy transfer would allow both better apprehending microstructural changes in irradiated materials and precise tailoring of ion-beam-induced material modifications.

To address this topic, silicon carbide (SiC) is a ceramic material that is perfectly suited. Indeed, it exhibits a subtle behavior with respect to irradiation-induced damage accumulation: defect creation and annihilation rates intimately depend on the irradiation conditions and also on the presence of atomic-arrangement disturbances (see, e.g., [3–7]). Besides this property that is relevant for fundamental studies of ion/solid interactions, SiC has been attracting an increasing interest for technological applications. These latter usually involve harsh radiative environments: structural components in fission and fusion reactors [8], devices for high-power microelectronic and spintronic applications [9] for which ion (beam) doping is required. This later field includes devices for space exploration, and in that case, SiC can experience catastrophic failure due to the so-called single-event burnout phenomenon arising from highly ionizing particle irradiation [10]. Therefore, during its synthesis and/or actual use, SiC is, or will be subjected to ion irradiation. Increasing the body of knowledge regarding its response to intense energy deposition, as can occur in the above-mentioned instances, thus appears as a major issue to tackle.

It is recognized that SiC readily undergoes amorphization when irradiated in the nuclear energy-loss (S_n) regime (hundreds of keV) for which projectile energy is transferred to the target (screened) nuclei. This process is complete at a few tenths of displacement per atom (dpa) at room temperature (RT) [3–5]. Increasing (decreasing) irradiation temperature leads to an increase (decrease) in the required dpa level for a total phase transformation, and amorphization can even be suppressed above a few hundreds of degrees Celsius [3,4]. In contrast, SiC irradiated in the electronic energy-loss (S_e) regime (hundreds of MeV), for which projectiles first transfer their energy to target electrons (and subsequently to the atomic network through electron-phonon coupling), exhibits very little disordering, as only production of point defects has been observed [6]. Interestingly, in SiC initially disordered by irradiation in the S_n regime, damage recovery has been shown to occur when the material was subsequently irradiated in the S_e regime. This phenomenon was observed upon swift heavy ion (SHI) irradiation in the GeV energy range at RT [11] and has been called SHIBIEC, which stands for swift heavy ion-beam-induced epitaxial recrystallization. It has been ascribed to the intense electronic energy (hereafter also referred to as ionization process) deposited by SHIs, and a thermal spike effect has been invoked to account for this process [5,12]. The recovery was found to be dependent on the initial damage

state. In fully amorphous (FA) layers, recrystallization takes place at the buried amorphous-crystalline (a-c) interface. In partially amorphous (PA) samples (i.e., where amorphous regions are surrounded by defective but still crystalline regions), the recovery occurs over the entire damaged thickness. This healing phenomenon has also been observed in disordered SiC crystals irradiated with (different) ions of intermediate energy (in the MeV range) [13], i.e., with a lower S_e component (a few keV/nm vs ∼30 keV/nm). Recovery cross sections have been determined and, though they depend on the initial disorder level, they typically lie in the range of a few square nanometers [13,14]. In the above-mentioned studies, both sequential ($S_n + S_e$, i.e. SHIBIEC) and simultaneous ($S_n\&S_e$, referred to as the SNEEL effect, which stands for synergy between electronic and nuclear energy loss, see [15]) irradiation experiments have been performed. In these two cases, a recovery has been measured when combining S_n and S_e, although the two energy deposition processes are uncoupled (in time and space). Very recently, a coupled effect, i.e., with $S_n\&S_e$ delivered by the same ion, on disorder accumulation has been demonstrated with ions in the MeV range [16]: the damage creation rate has been found to decrease with increasing the S_e/S_n ratio.

Although the understanding of the ionization-induced defect recovery phenomenon is progressing, some questions remain to be addressed. In particular, the combined effect of temperature and electronic energy deposition is a major subject to tackle, because for most of its potential or actual applications, SiC is subjected to both irradiation and temperature. Furthermore, acquisition of new data should allow for a better description of the recovery mechanism. This question has not been addressed so far, except very recently by Hlatshwayo *et al.*, who studied the effect of SHI irradiation at 773 K on amorphous SiC [17]. They put forward an enhanced annealing effect with respect to a sole thermal annealing at the same temperature.

In the present paper, we report a study dedicated to the combined effect of irradiation temperature and electronic energy deposition. We first present molecular dynamics (MD) data that are supposed to predict effects of the SHI irradiation temperature on the recovery process efficiency (in the 100–800 K range). These results are then verified and complemented by a series of systematic irradiation experiments where the initial disorder level, the SHI fluence, and the irradiation temperature are varied. Rutherford backscattering spectrometry in channeling mode (RBS/C) was used to monitor the disorder level in irradiated crystals, and a transmission electron microscopy (TEM) investigation was carried out to characterize their microstructure. A two-step scenario of defect annealing is proposed.

II. MOLECULAR DYNAMICS PREDICTIONS OF ELECTRONIC ENERGY DEPOSITION AT VARIOUS TEMPERATURES

A. Methodology of damage creation and of electronic energy deposition

The methodology implemented to model the effect of the intense electronic energy deposition on the defective SiC lattice is fully described in [12,16]. In the following, we briefly provide the major details and above all, the corresponding results. The molecular dynamics code PARCAS [18] was used to both create the disordered SiC cells and to simulate the electronic energy loss. Si-C interactions were described by the Gao-Weber potential [19]. The predamaged state was produced by introducing 0.1% of Frenkel pairs in a pristine MD simulation cell. While this defect concentration is low, it is sufficient to provide qualitative trends in the subsequent disorder recovery. Introducing a larger defect density would require a significantly higher computing time without providing additional crucial information (unless a systematic analysis that takes into account the defect features is undertaken). Energy deposited into the electronic subsystem leads to highly excited electrons along the ion track (i.e., a cylinder) which rapidly (<0.5 ps) distribute their energy through electron-electron interactions, and subsequently (∼0.5–10 ps) transfer their energy via electron-phonon coupling to the atomic subsystem. The most widely used approach to treat these energy transfers is the two-temperature model (2T model), which considers both subsystems as a coupled continuous medium [16,20]. To simulate the local heating from the electronic energy loss (∼33 keV/nm, see Sec. III), the radial and temporal distributions of the atomic temperature were estimated from the inelastic thermal spike model derived from solutions of the 2T model [20] (see Fig. 1). Parameters (such as thermal conductivity and electron-phonon coupling strength) used in this study are given in [16]. It is to be mentioned that, as the initial defect concentration was chosen to be low, values for perfect SiC were used. Figure 1 markedly shows that the temperature inside the track reaches very high values, larger than 4000 K. After 5 ps, a duration corresponding to more than 100 lattice vibrations in SiC, the temperature still exceeds 2000 K within a 2-nm distance from the track core, i.e., a distance close to 10 times the first-nearest-neighbor average distance. Defect annealing being a thermally activated process, it is easily conceivable that such a high temperature can induce lattice recovery. This effect is studied hereafter.

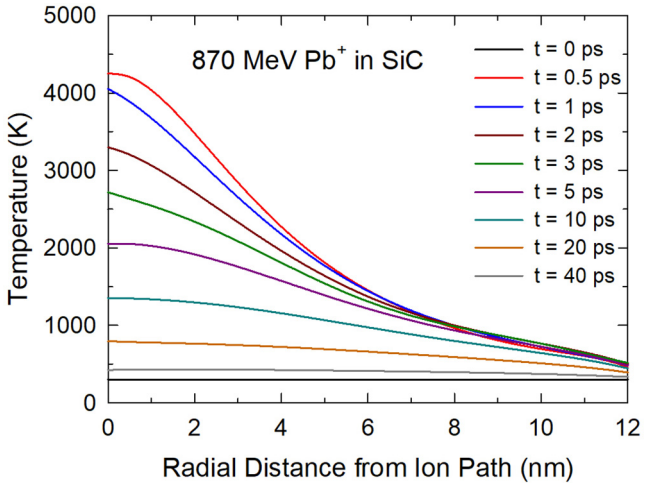

FIG. 1. Simulations, in the framework of the inelastic thermal spike model, of the radial and temporal distributions of the atomic temperature during 870 MeV Pb ion irradiation in SiC.

B. Effect of electronic energy deposition on disorder level

The structure of the damaged simulation cells was analyzed after ion impacts by a structure factor method where defects are defined based on deviation from the bond angles in the ideal zinc blende structure of 3C-SiC. Note that ions directly overlapped, meaning that the exact same location and direction were selected for the ions to hit the simulation cell. This solution prevents any direct comparison with an actual ion fluence, but as qualitative results were expected from these MD simulations, it has the advantage of being less costly in computing time. The evolution of the relative disorder as a function of overlapped ions and temperature is presented in Fig. 2(a). The macroscopic temperature in different sets of simulations was varied from 100 to 800 K by preparing the initial cells at those temperatures with a short *NPT* relaxation run before the ion track simulations. The macroscopic temperature was also used for the boundary cooling during the ion track simulations and for the 120-ps relaxation runs between each track. The initial disorder is necessarily 1.0 for all temperatures, because we plotted the relative disorder, i.e., the disorder normalized to the initial defect level. The disorder markedly decreases with increasing the number of SHI impacts, irrespective of the temperature. On the contrary, the higher the temperature, the lower the residual disorder. Computed data were fitted using a double exponential decay function (using a single exponential did not allow for a correct data fitting). The reason as to why two different active recovery processes are required is unclear. Yet, it can be assumed that two main types of defects having lower and larger activation energy, such as point defects and small defect clusters, respectively, are being annealed with different rates. No clear progression emerged from the variation of the recovery cross sections with temperature. Contrarily, the relative recovery rate (i.e., the normalized decrease in disorder) is doubled (15%–30%), going from 100 to 800 K. We have also simulated isothermal annealing at 800 K on the same time scale as the thermal spikes (i.e., disorder measured every 120 ps) for comparison, and the results, shown in Fig. 2(b), demonstrate some recovery over the time scale of individual thermal spikes. However, the thermal recovery is substantially less than that induced by the 870-MeV Pb ions at 800 K.

From the MD results, it appears that changing the irradiation temperature should affect the recovery efficiency, with a more pronounced annealing rate at higher temperature. This result seems to be obvious. Nonetheless, it deserves to be discussed. Indeed, as shown with the thermal spike calculations, the local increase in temperature due to the intense ionization process is tremendous (a few thousand degrees) as compared to the change in macroscopic temperature. Therefore, it can be surprising to observe a reduced annealing rate at 100 K. Similarly, with increasing temperature, one could think that defect mobility is enhanced and thus defect recombination is promoted. However, it has been shown that during a thermal treatment above 540 K, in the case of weakly damaged SiC (i.e., close to that of the current initial MD cell), most of interstitial defects cluster and thus become immobile [21]. Therefore, increasing the temperature at 800 K could prevent defect annealing (even though Si vacancies may become mobile around ∼700 K [22]). In fact, defect interactions with

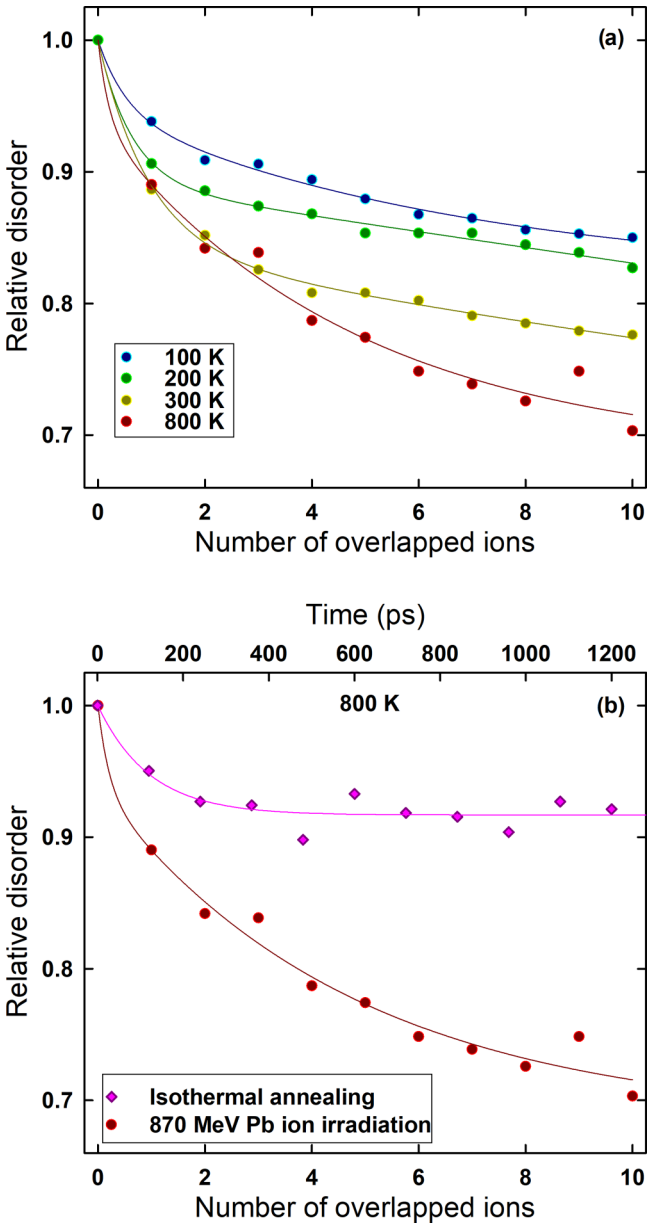

FIG. 2. Variation of the MD-derived relative disorder in SiC as a function of (a) the number of overlapped SHIs and for different temperatures (see labels) and (b) the number of overlapped SHIs and the time for both SHIs and thermal annealing. Lines are fits to experimental data using a double exponential decay function.

changing irradiation temperature [2,3] or dose [2,3,5] as well as particle energy deposition [5–7,13,15] are quite complex in SiC and consequently, experimental evidence of the current MD predictions should be provided. This is the purpose of the next sections.

III. EXPERIMENTAL DETAILS

A. SiC single crystals and irradiation conditions

The {0001}-oriented 6H-SiC single crystals, provided by MTI Corporation (Richmond, VA, USA), were in a first step irradiated with the IRMA ion implanter of the SCALP facility

TABLE I. Characteristics of the studied SiC crystals. Φ_{Fe} is the Fe fluence, T_{Pb} is the Pb irradiation temperature, and f_D^{max} is the disorder at the damage peak as determined from the MCCHASY simulations of the RBS/C spectra. The other terms are fitting parameters used in Eqs. (1) and (2). FA means fully amorphous and PA stands for partially amorphous; PA-1 and PA-2 correspond to two different initial disorder levels.

$\Phi_{Fe}(cm^{-2})$	Name	T_{Pb}	f_D^{max}	$f_D^{int\,eg,\,init}$	$f_D^{int\,eg,\,min}$	$\sigma(nm^2)$	$\tau^{max}(\%)$
4×10^{14}	FA	LT	1 ± 0.02	100	N/A	N/A	N/A
4×10^{14}	FA	HT	1 ± 0.02	100	N/A	N/A	N/A
2.2×10^{14}	PA-1	LT	0.95 ± 0.02	0.57 ± 0.03	0.34 ± 0.02	1.5 ± 0.4	40 ± 2
2.2×10^{14}	PA-1	HT	0.95 ± 0.02	0.57 ± 0.03	0.26 ± 0.01	1.8 ± 0.2	54 ± 2
1.8×10^{14}	PA-2	LT	0.83 ± 0.03	0.46 ± 0.05	0.18 ± 0.02	1.6 ± 0.4	60 ± 4
1.8×10^{14}	PA-2	HT	0.83 ± 0.03	0.45 ± 0.05	0.11 ± 0.01	3.3 ± 0.6	75 ± 2

[23], with 100 keV Fe^+ ions at RT to fluences of 1.8×10^{14}, 2.2×10^{14}, and 4×10^{14} cm^{-2} (corresponding to ~0.32, ~0.4 and ~0.71 dpa, as calculated with SRIM [24], see [5] for details). The ion flux was kept constant and low (a few 10^{11} cm^{-2} s^{-1}) to avoid excessive heating. In addition, as the damage accumulation rate depends on the ion flux, keeping this parameter constant was a mandatory condition to create three effectively different microstructures (i.e., one for each Fe fluence).

In a second step, these damaged crystals were irradiated with 0.87 GeV Pb ions at the GANIL facility in Caen (France) at both ~100 and ~770 K, hereafter referred to as low temperature (LT) and high temperature (HT), respectively. Temperature was monitored using a thermocouple located as close as possible to the samples. Three fluences of SHIs, 7.5×10^{12}, 2×10^{13}, and 4×10^{13} cm^{-2}, were used in order to vary the amount of deposited electronic energy. For this high ion energy, as determined with SRIM calculations [24], ballistically induced displacement damage is negligible because the nuclear energy loss is <0.1 keV/nm (with a maximum of 2×10^{-3} dpa), and this latter is much weaker than the electronic energy loss that has a value of 33 keV/nm over a thickness of nearly 20 μm. In both low- and high-energy irradiation experiments, crystals were tilted off any major axial or planar direction during irradiation to limit channeling effects. Characteristics and labels of the samples are provided in Table I.

Note that experiments have been carried out on 6H-SiC, whereas MD simulations were performed on 3C-SiC. However, the simulations were meant to provide some predictive trends, not to precisely fit with experiments. In addition, although some differences in defect energetics exist between the two polytypes, it has been shown that they both behave similarly, at a mesoscopic scale, under low- and high-energy irradiation [5,7,11,14,25].

B. Sample characterizations

Rutherford backscattering spectrometry in channeling condition was performed using a 1.4-MeV He^+ ion beam delivered by the ARAMIS accelerator of the SCALP platform at CSNSM [23]. Experimental spectra were fitted using the MCCHASY Monte Carlo code developed at the National Center for Nuclear Research (NCBJ) in Warsaw [26]. In this work, the disorder is accounted for by considering that a fraction of atoms, f_D, are randomly displaced from their regular crystallographic site. Since amorphization in SiC irradiated at RT proceeds via the formation of point defects that cluster to form amorphous regions (no extended defects such as dislocation loops are formed), this assumption is perfectly reasonable. High-resolution TEM characterizations were also carried out on three selected samples using a microscope operated at 200 keV (JEOL 2010F).

IV. RBS/C AND TEM CHARACTERIZATIONS

A. RBS/C results

Figures 3(a)–3(c) and 4(a)–4(c) present the Si signal of RBS/C spectra recorded on 6H-SiC single crystals predamaged with 100 keV Fe^+ ions at RT and subsequently irradiated with 0.87 GeV Pb ions at LT (Fig. 3) and HT (Fig. 4). The spectrum recorded in the ⟨0001⟩ axial direction on a pristine crystal is also plotted [crosses in Fig. 2(a)], and it shows a very low backscattering yield (as compared to the random one, stars) on the entire analyzed thickness. This finding attests to the very good quality of the single crystals used for this study. Upon Fe irradiation (black symbols in all figures), the backscattering yield in the axial direction increases around 750 keV with increasing the Fe fluence, which means that the crystal is damaged at the corresponding depth. At the highest Fe fluence of 4×10^{14} cm^{-2}, the aligned yield reaches the random level, a result that shows that the crystals have been amorphized by Fe irradiation (as already observed in [5,7]). The RBS spectra recorded in the ⟨0001⟩ axial direction after swift Pb ion irradiation only [gray circles in Figs. 3(a) and 4(a)] indicate that little damage is created by swift ion irradiation alone, even at low temperature [see Fig. 3(a)]. The effect of SHI irradiation on the predamaged crystals (colored symbols) appears as (i) a shrinkage of the fully amorphous (FA, see Table I) layer [see Figs. 3(a) and 4(a)] or (ii) a decrease of the backscattering yield in the damage region for partially amorphous (PA, see Table I) layers [Figs. 3(b) and 3(c), and Figs. 4(b) and 4(c); these effects are more pronounced with increasing the Pb ion fluence. This difference between the two initial disorder levels was previously evidenced [7,14]. In contrast, a new result is the effect of the SHI irradiation temperature: the higher the irradiation temperature, the more pronounced the recovery process.

All RBS/C spectra displayed in Figs. 3 and 4 (a, b, and c) were fitted (solid lines) by using Monte Carlo simulations performed with the MCCHASY computer code [26]. Figures 3 and 4 (d, e, and f) show the corresponding disorder depth profiles (variation of f_D in the Si sublattice as a function of the depth)

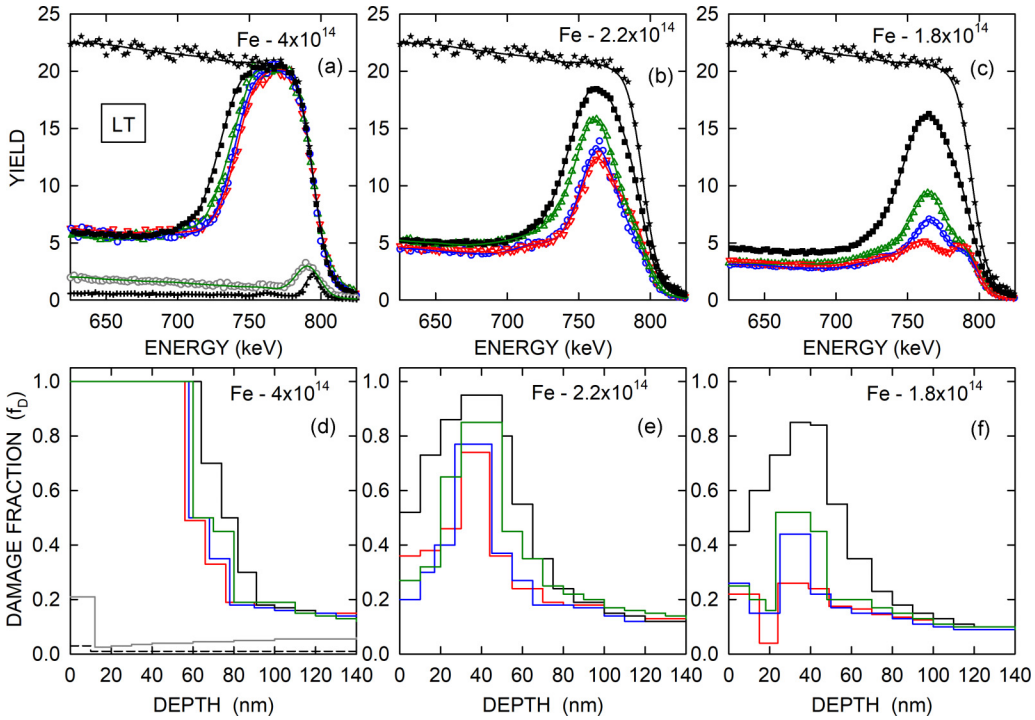

FIG. 3. (a, b, c) RBS spectra (Si signal) recorded along the ⟨0001⟩ direction for 6H-SiC single crystals first damaged by 100 keV Fe^+ ions at RT at the indicated fluences (black squares) and subsequently irradiated with 0.87 GeV Pb ions at ∼100 K (LT) at $7.5 \times 10^{12}\,cm^{-2}$ (green, up triangles), $2 \times 10^{13}\,cm^{-2}$ (blue circles), and $4 \times 10^{13}\,cm^{-2}$ (red, down triangles). Also plotted are spectra recorded in a random direction (stars) and along the ⟨0001⟩ direction for a pristine crystal (crosses). Gray circles correspond to a pristine crystal irradiated with 0.87 GeV Pb ions at $4 \times 10^{13}\,cm^{-2}$ at LT. Solid lines are fits to experimental data with the MCCHASY code [26]. (d, e, f) Damage fraction (f_D) as a function of the depth extracted from the fits to experimental RBS/C data for 6H-SiC single crystals damaged by 100 keV Fe^+ ions at RT at indicated fluences (black lines) and subsequently irradiated with 0.87 GeV Pb ions at LT at $7.5 \times 10^{12}\,cm^{-2}$ (green lines), $2 \times 10^{13}\,cm^{-2}$ (blue lines), and $4 \times 10^{13}\,cm^{-2}$ (red lines). The dashed black line corresponds to the pristine crystal and the gray solid line to the crystal irradiated with SHIs at $4 \times 10^{13}\,cm^{-2}$ at LT.

for both LT and HT irradiations, respectively. A rather narrow damage peak is exhibited at around 30–40 nm for samples predamaged with Fe^+ ions at 1.8 and $2.2 \times 10^{14}\,cm^{-2}$ (black lines), with a maximum disorder level that increases with increasing ion fluence. At an Fe fluence of $4 \times 10^{14}\,cm^{-2}$, f_D reaches 1 over a thickness of ∼65 nm, indicating that the crystal has been amorphized from the surface up to this depth. The disorder depth profile of SiC irradiated only with SHIs at both low and high temperature is rather flat, with a very low disorder level close to that of a pristine crystal (however, decreasing the irradiation temperature leads to a slightly higher degree of disorder than at high temperature).

Figures 3 and 4 (d, e, and f) also show the disorder profiles obtained after irradiation with swift Pb ions of predamaged samples (colored lines). Consistently with the raw RBS/C data, the results show: (i) a shrinkage of the FA layer for amorphized samples (e.g., from ∼65 to ∼55 nm after irradiation at $4 \times 10^{13}\,cm^{-2}$ at LT), (ii) a decrease of f_D for PA layers, with the higher the SHI fluence, the larger the recovery, i.e., the lower the final disorder level f_D^{min} (e.g., from 0.85 to 0.25 after Fe irradiation at $1.8 \times 10^{14}\,cm^{-2}$ and Pb irradiation at $4 \times 10^{13}\,cm^{-2}$ at LT). Starting from a same disorder level or amorphous thickness, the increase in SHI irradiation temperature (100–770 K) leads to a more pronounced annealing effect. A quantitative analysis of these data is presented in Sec. V.

To finish with the RBS/C findings, it is important to mention the results (detailed hereafter but not shown for the sake of simplicity) that we obtained for predamaged SiC crystals that were thermally treated at only ∼770 K in order to determine the effect of the thermal load on the crystal recovery (independently of the SHI irradiation). Although it has not been possible to use the same device as the one present in the irradiation chamber, we tried to reproduce at best the conditions that the SHI-irradiated samples experienced, i.e., an annealing during 15 h at ∼770 K. We also performed an annealing at ∼770 K but during 8 h only. We measured in both cases a significant crystal recovery, and the disorder at the remaining damage peak was found to be very close to that determined after SHI at HT. We will comment these results in Sec. V.

B. TEM results

In order to get a better representation of the microstructure associated with the predamaged and SHI-irradiated crystals, we performed a transmission electron microscopy analysis. Images are presented in Fig. 5. For the layer irradiated with Fe ions at $1.8 \times 10^{14}\,cm^{-2}$ (PA-2), high-resolution TEM shows [Fig. 5(a)] that the crystalline disturbances are not uniform along the surface normal. A crystalline, disordered region is observed on both parts of a damage peak that consists of a nearly completely amorphous region, as evidenced by both

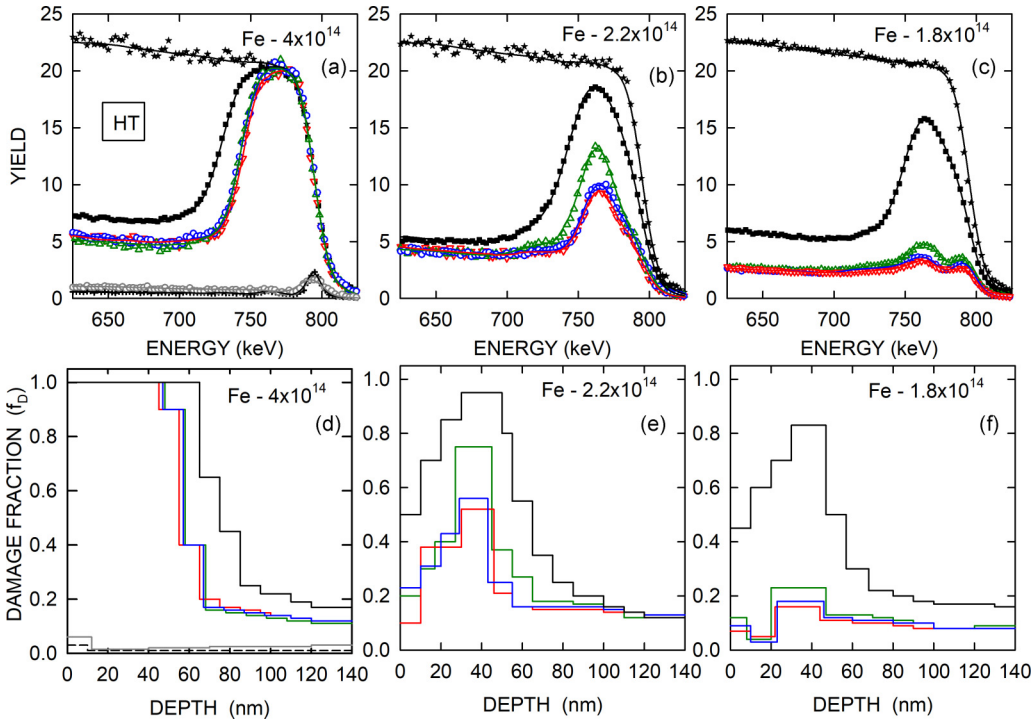

FIG. 4. Same captions as for Fig. 3 but for 6H-SiC single crystals irradiated with 0.87 GeV Pb ions at HT (∼770 K).

the typical contrast on the bright-field image and the corresponding Fast Fourier transform (FFT) that shows essentially one central spot surrounded by diffuse scattering. Beneath the damaged area, there is a pristine region, as attested by the high-resolution TEM image with perfect atomic rows parallel to the (0001) planes and by the FFT that reveals multiple aligned spots. It is worth noting that the disorder profile obtained by RBS/C (red line) matches that of the TEM (after adapting the depth scale to account for the change in the density, see [14] and references therein). After SHI irradiation at LT at a fluence of 4×10^{13} cm^{-2} [Fig. 5(b)], the layer exhibits a similar but less disordered microstructure with remaining but less dense amorphous regions surrounded by crystalline disordered regions. The FFT exhibits more intense spots (along the central line), supporting the conclusion of a higher crystalline quality. After SHI at HT (at 4×10^{13} cm^{-2}), the SiC layer shows a different microstructure [Fig. 5(c)]. Although the TEM image is contrasted, it is clearly less blurred, suggesting that very few amorphous regions survived; the corresponding FFT readily resembles that of the pristine region, although the spots are slightly more diffuse. Therefore, a significant fraction of the disorder has been annealed.

V. DISCUSSION

A. Summary of RBS/C results: Assessment of the temperature effect on the recovery process

As shown in the previous sections, the effect of SHI irradiation on the disorder level depends on both the initial damage state and the temperature. In order to better highlight this

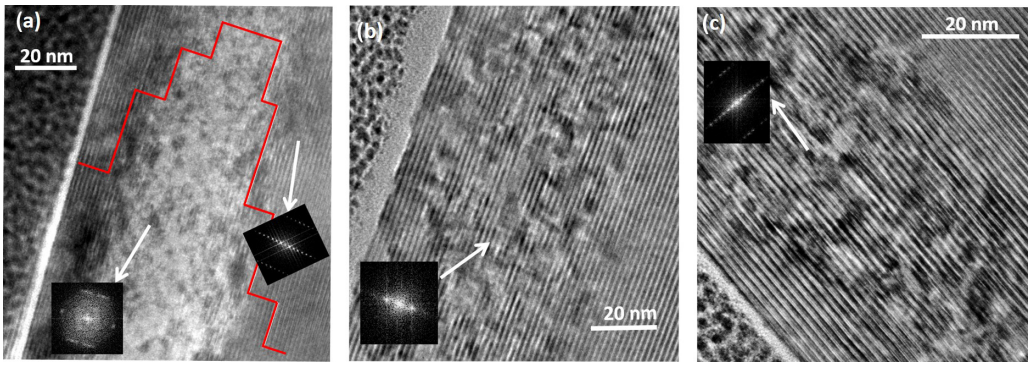

FIG. 5. HRTEM images recorded with {0001} planes perpendicular to the surface for 6H-SiC crystals irradiated with (a) Fe ions at 1.8×10^{14} cm^{-2}, (b) Fe ions at 1.8×10^{14} cm^{-2} and Pb irradiation at 4×10^{13} cm^{-2} at ∼100 K, and (c) Fe ions at 1.8×10^{14} cm^{-2} and Pb irradiation at 4×10^{13} cm^{-2} at ∼770 K. Insets present the fast Fourier transforms (FFTs) of some selected regions. The red line in Fig. 5(a) corresponds to the disorder profile determined by RBS/C, see Fig. 4(f).

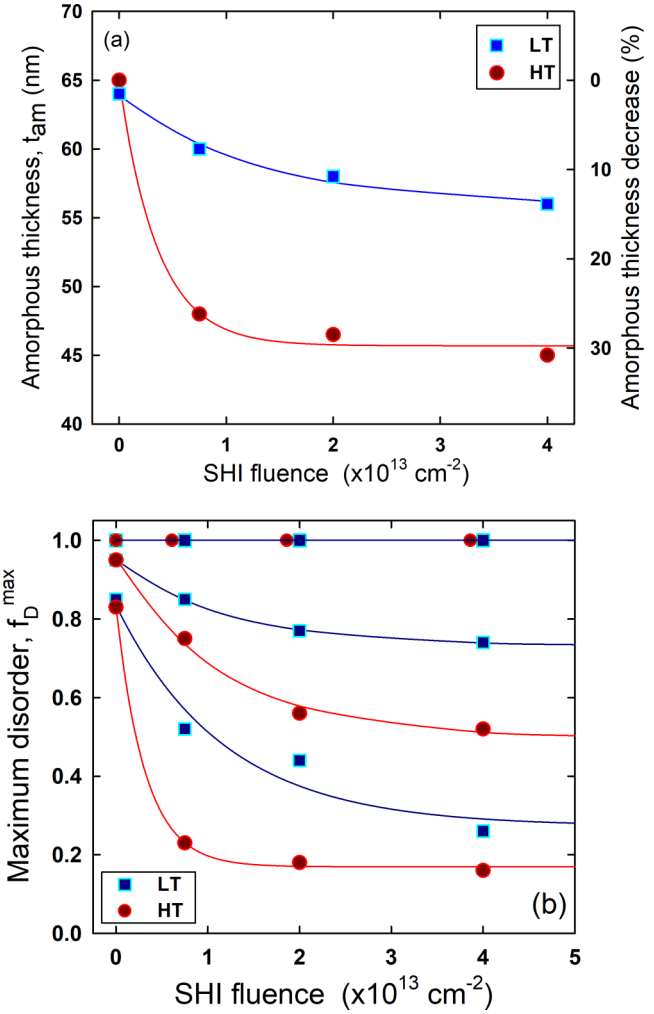

FIG. 6. (a) Variation of the thickness of the amorphous layer (t_{am}) and (b) variation of $f_D{}^{max}$ (i.e., f_D determined at the damage peak) as a function of the swift Pb ion fluence for 6H-SiC single crystals damaged by 100 keV Fe^+ at RT and subsequently irradiated with 0.87 GeV Pb ions at LT (blue squares) or HT (red circles). Lines are drawn for visualization purposes.

statement and to get quantitative information on the recovery process, we plotted the variation of the amorphous thickness (t_{am}) for FA layers and that of the disorder level at the damage peak (f_D^{max}) for PA layers as a function of the SHI fluence for both LT and HT.

We first consider the case of FA irradiated layers. Figure 6(a) presents the variation of t_{am} as a function of the Pb ion fluence for LT and HT irradiations. A decrease in the amorphous thickness is markedly observed for the two temperatures of approximately 12% and 30% for LT and HT, respectively. These values show that increasing the SHI irradiation temperature enhances the recrystallization at the interface. In a recent study, where polycrystalline predamaged SiC samples were irradiated at 773 K with SHIs (167 MeV Xe at 5×10^{13} cm^{-2}), authors also reported a shrinkage of the amorphous layer [17]. This latter was measured by TEM and was found to be between 7% and 13%, depending on the predamaging conditions (360 keV I or Kr, respectively). Even taking into account the decrease in density of amorphous SiC with respect to crystalline SiC (which would lower the decrease in size of the amorphous layer that we measured by RBS/C assuming the density of crystalline SiC), the annealing observed in the present work appears to be more important than that determined by Hlatshwayo and co-workers [17]. This difference can be due to (i) a nonequivalent initial amorphous state (the amorphous structure depends on the irradiation conditions in SiC [27]), (ii) the duration of the thermal treatment, and (iii) the larger energy deposited by 0.87 GeV Pb ions than by 167 MeV Xe ions (33 keV/nm vs 20 keV/nm).

Now we focus on the two sets of PA layers. In Fig. 6(b) is plotted the variation of f_D^{max} as a function of the Pb ion fluence for both LT and HT, and for the two initial damage states. Increasing the irradiation temperature allows a higher recovery rate, which means that a lower disorder level is obtained after 770 K Pb irradiation than after 100 K irradiation. Nevertheless, interestingly, the healing does occur even at very low temperature, most likely because it is majorly due to the intense electronic energy deposition. This result is in contrast with the IBIEC process, for which a temperature of a few hundred degrees Celsius is required to promote defect migration initiated by nuclear energy deposition [28,29], and also with dynamic annealing that takes place in SiC for irradiation above ∼470 K [2,30].

These experimental results are in agreement with the findings obtained by MD simulations shown in Fig. 2(a), which predicted a change in the recovery efficiency with varying the temperature. This agreement indicates that the methodology of combining MD simulations and the thermal spike model is relevant to describe the recovery mechanism, at least to capture the qualitative trends of this phenomenon. In this regard, two important results can be put forward: (i) ionization-induced annealing takes place at a temperature as low as 100 K, and (ii) the irradiation temperature significantly affects the recovery efficiency. This second point was already shown in [17], although, as in the current study, it is difficult to precisely determine the separate contributions of the thermal load and of the ionization process on crystal recovery when the SHI irradiation is performed at HT. These two major results lead to two questions. First, why is an annealing effect observed at LT irradiation? Indeed, at 100 K, the majority of defects in SiC are immobile and thus highly stable [22,31]. A likely explanation is that the tremendous temperature reached in the ion track (see Fig. 1) allows some of these defects to overcome their migration barrier [22,31] and thus to be annealed (or to adopt a new configuration). But this explanation leads to a second question: Why does a minor variation in the macroscopic temperature with respect to that reached in the ion track (i.e., a few hundred vs a few thousand degrees) induce such a noticeable change in the ionization-induced recovery efficiency? The quantitative analysis provided hereafter brings additional information to answer this question and sheds light on the overall ionization-induced mechanism.

B. Quantitative analysis: Insights into the recovery phenomenon

As previously shown in [14], the recovery cross section calculated from the variation of the disorder level determined exclusively at the damage peak may not reflect the actual

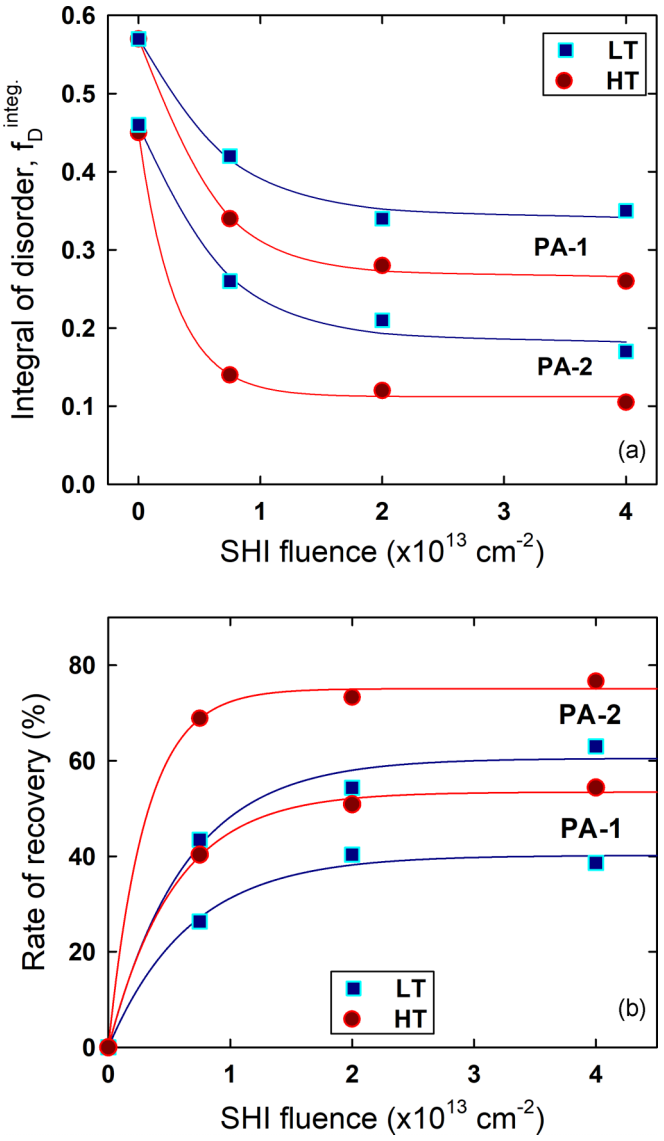

FIG. 7. (a) Variation of $f_D^{\text{int } eg}$ (i.e., f_D integrated over the disorder profile and normalized to the initial disorder) as a function of the swift Pb ion fluence for 6H-SiC single crystals damaged by 100 keV Fe^+ at RT and subsequently irradiated with 0.87 GeV Pb ions at LT (blue squares) or HT (red circles). Lines are fits to experimental data using Eq. (1). (b) Same caption as in (a) but for the rate of recovery τ.

overall healing that takes place upon irradiation. Indeed, recovery occurs over the entire damage layer, and restricting the analysis to the peak neglects the contribution of the less disordered regions. Therefore, to realize a thorough quantitative analysis of the recovery process, we determined the variation of the relative integrated disorder (i.e., over the entire damage profile). This latter is plotted in Fig. 7(a). The trend in the experimental data shows an exponential decrease in the disorder with an asymptotic behavior, so we used the following equation to fit these data:

$$f_D^{\text{int } eg} = \left(f_D^{\text{int } eg,\ \text{initial}} - f_D^{\text{int } eg,\ \text{min}}\right) \exp\left(-\sigma\,\Phi_{Pb}\right) + f_D^{\text{int } eg,\ \text{min}}. \tag{1}$$

In this equation, Φ_{Pb} is the Pb ion fluence, σ corresponds to the average recovery cross section, $f_D^{\text{int } eg,\ \text{initial}}$ is equal to the integrated disorder level prior to SHI irradiation, and $f_D^{\text{int } eg,\ \text{min}}$ represents the minimum value of the (integrated) disorder level that can be reached after SHI irradiation. We also calculated the rate of recovery, τ, i.e., the rate of disorder annealing as a function of the Pb ion fluence and irradiation temperature [Fig. 7(b)]. These data follow a similar (but necessarily opposite) trend to that of the variation of the relative integrated disorder, and it can be described by the following equation, with $\tau^{\max}$ being the asymptotic (final) recovery rate:

$$\tau = \tau^{\max}[1 - \exp(-\sigma\,\Phi_{\text{Pb}})]. \tag{2}$$

The fitting parameters $f_D^{\text{int } eg,\ \text{initial}}$, $f_D^{\text{int } eg,\ \text{min}}$, σ, and $\tau^{\max}$ are reported in Table I [note that σ is obviously identical in Eqs. (1) and (2)].

For layers close to full amorphization (PA-1, $f_D^{\max} = 0.95$), average recovery cross sections in the range ~1.5–1.8 nm^2 are found. These values are similar to those determined in the case of SiC crystals (i) irradiated at RT with ions having a 5 keV/nm electronic energy loss (21 MeV Si), i.e., much lower than the 33 keV/nm for the present study, (ii) but initially exhibiting a lower disorder level at the damage peak (0.72 vs 0.95) [13,16]. This finding suggests, as for the comparison with the work of Hlatshwayo *et al.* [17], that the level of deposited electronic energy influences the recovery efficiency. The recovery cross section for these severely disordered layers does not seem to depend on the irradiation temperature. The minimum disorder level is, however, found to be much lower for irradiations at 770 K, a result that is illustrated in Fig. 7(b), showing final rates of recovery $\tau^{\max} \sim 39\%$ and $\sim 54\%$ for the LT and HT irradiations, respectively. The comparable recovery cross sections suggest that some of the defects are first rapidly annealed due to the electronic energy deposition, and the change in the macroscopic temperature does not, in this case, affect this process. The higher rate of recovery (i.e., lower $f_D^{\text{int } eg,\ \text{min}}$) after irradiation at HT can be due to additional defect annealing arising from the thermal energy brought during the (long) thermal load. The annealed defects could have been initially present (considering that the defective layers contain a wide defect spectrum that includes antisites, point and clustered defects, amorphous regions) or generated during the cooling down phase subsequent to the thermal spike.

For less disordered layers (PA-2, $f_D^{\max} \sim 0.85$), the recovery cross section upon irradiation at LT, i.e., $\sim 1.6 \pm 0.4$ nm^2, is only slightly larger than for the more disordered layers (PA-1), i.e., $\sim 1.5 \pm 0.4$ nm^2. This finding suggests that this cross-section value is essentially governed by the annealing of the same, least stable defects that are first annealed, irrespective of the initial damage state. However, this latter affects the final disorder level. Indeed, the curve of the recovery rate for the PA-2 layers irradiated at LT is very close to that for the PA-1 layers irradiated at HT [see Fig. 7(b)]. In other words, it seems that the beneficial effect on the recovery efficiency of an increase in temperature is compensated by the detrimental effect of a higher initial disorder (or reciprocally, the beneficial effect of a lower disorder level is counterbalanced by a lower irradiation temperature). The final recovery rate at the

two temperatures but for a same initial disorder (PA-2 layers) is found to be ∼60% and 75% for LT and HT irradiations, respectively. As for the PA-1 layers, increasing the irradiation temperature leads to a more pronounced recovery. It is in addition worth mentioning that the rather small difference between these two recovery rates is in fact related to a dramatic change in the microstructure, which is illustrated by the TEM analysis: after irradiation at LT, there remain amorphous regions [Fig. 5(b)], while for HT irradiation [Fig. 5(c)] such defects almost completely disappeared. Finally, it must be noted that the recovery cross section for PA-2 layers irradiated at HT is twice (3.3 nm^2 vs 1.8 nm^2) that observed for the same initially damaged layer but irradiated at LT. This result (although relying on only one data point) suggests that in addition to thermodynamics considerations, i.e., defect migration barriers to be overcome for defect annealing to occur, the kinetics of defect reactions should also be invoked. More explicitly, the first Pb ion fluence was reached after about 3 h, so during this time, numerous defects in the less defective layer could have been annealed out during the irradiation at 770 K because of the thermal load itself. Indeed, at this temperature it was shown that a few seconds to a few minutes only are required to reach a steady state [32,33]. On the contrary, in the heavily defective layer (PA-1), 3 h were not sufficient to lead to a substantial recovery process. This statement is supported by results that showed that annealing at 1073 K for 2 h led to a slight decrease in disorder in an irradiated layer with a damage peak of 0.7 [34], i.e., at higher temperature and with a lower initial disorder level than in the current work. Of course, at low temperature, the duration of the thermal treatment is irrelevant as the defects are not mobile [22,32].

C. Recovery process: A tentative two-step scenario

The overall results presented above lead us to propose that the recovery phenomenon taking place during SHI irradiation is a two-step mechanism with distinct but not independent processes. In a first step, the intense electronic energy deposition is transferred to the atomic subsystem, which leads to a thermal spike and to the formation of a track, i.e., a cylinder into which lattice as well as displaced atoms are given a tremendous energy [12,20]. This process can cause interstitial evaporation from clusters, thereby hindering cluster nucleation and growth as well as increasing the probability for some recombination of interstitials with vacancies; it may also enhance clustering and growth of dislocation loops, which can lead to a reduction in measured disorder using RBS/C (as observed in, e.g., [15]). From our TEM images, it does not seem that dislocation loops are formed, so it should be more likely that during the cooling phase of the thermal spike, part of the initial disorder is annealed through defect reactions such as interstitial-vacancy recombination and antisite elimination. In a second step, defects in a metastable state, either initially present or formed during the cooling phase of the thermal spike, can be annealed out owing to the thermal energy associated to the thermal load. This second step is likely, in SiC, insignificant at 100 K, already active at RT, and favored at 770 K. It occurs over a longer timescale than the thermal spike event. Indeed, as shown in Fig. 2(b), only a small annealing effect is observed in the microsecond range, i.e., a time several decades larger than the thermal spike duration; similarly, it has been recently demonstrated that typical relaxation time in SiC is in the range of the millisecond [35]. Both steps also differ in terms of length scale, as electronic energy is locally deposited whereas the irradiation temperature affects the whole sample. Nonetheless, the macroscopic temperature inherently affects the rise, duration, and fall of the thermal spike, as both the thermal conductivity and the electron-phonon coupling depend on the material temperature (and on the crystalline level as well). Besides, the rates of the numerous defect reactions that can take place during the cooling phase of the spike are also temperature dependent. These remarks indicate that the temperature has a complex effect on both steps of the proposed mechanism. It is, however, fair to mention that such an interplay between thermodynamics and kinetics was already pointed out in 1975 by Adda *et al.* in a seminal paper [36] and later in a review paper [37]. Although in [36] the authors were dealing with collision cascades and not with excitation/ionization processes, the same idea was put forward, as ion irradiation is an external force that induces, locally and in a short timescale, atomic movements, the system under such a solicitation is kept away from thermodynamics equilibrium until the external force is interrupted. As a consequence, the final (micro-) structural changes are the result of both athermal (ballistically induced) and thermally activated atomic displacements. A major difference is to be noted, however: the thermal spike characteristics are temperature dependent, in contrast to features of collision cascade events.

From all these conclusions, we can argue that there exists an ionization-activated, thermally assisted defect annealing (IATADA) process in SiC. This mechanism is related to the time and spatial dissipation scales of the deposited energy, to the energy partition into the SiC atomic and electronic subsystems, and to the macroscopic temperature that affects both the energy dissipation processes and the defect reaction rates. In the Introduction, we mentioned several works that reported ionization effects in SiC under various experimental conditions, and in each case, a combined effect of electronic and nuclear energy deposition was shown to lead to some defect annealing. It is proposed that the two-step mechanism discussed above also applies for these different works, irrespective of the irradiation conditions and sequences, and allows understanding the actual measured damage creation rates.

D. Interplay between electronic and nuclear energy deposition

As a last point, it should be mentioned that, in the last few years, the study of ionization effects on ballistically generated defects has (re)gained great interest, and many other materials than SiC have been shown to be sensitive to this process. One can cite insulators (e.g., a-SiO_2 [38], KTO [39]), semiconductors (e.g., AlN [40], Si [41], UO_2 [42]) and even metals (e.g., Ni-based alloys [43]). Depending on the material, several phenomena can take place upon ionizing conditions: (i) a dramatic change in the configuration of the preexisting defects (UO_2, Ni), (ii) an exacerbation of the disordering efficiency (KTO, AlN), and (iii) a defect annealing (a-SiO_2, Si). Note that these phenomena can sometimes happen at the same

time, such as annealing and change in defect configuration, as in UO_2 and Ni alloys, for instance. This remark points out the complexity of the combined nuclear and electronic energy deposition effects on materials. Besides, the role of the sole irradiation temperature can be opposite according to the energy-loss regime and to the material. For instance, in cubic zirconia, increasing the temperature accelerates the disordering process in the nuclear energy-loss regime because defect clustering is enhanced [44], whereas damage accumulation is reduced in the electronic energy-loss regime owing to lower transient temperatures reached inside the SHI tracks [45]. All these results emphasize the intricate roles of the energy deposition and dissipation processes and of the temperature on the final microstructural state of irradiated materials. They also point out that systematic studies on various materials of different classes are required to provide enough data for a comprehensive, and potentially predictive description of the irradiation-induced effects in the materials during their aging.

VI. CONCLUSION

SiC single crystals, predamaged at different disorder levels in the nuclear energy-loss regime, were subsequently submitted to swift heavy ion irradiation at both low (∼100 K) and high (∼770 K) temperature in order to determine the effect of this parameter on the ionization-induced defect annealing generated by the SHIs. The deposited electronic energy allows reducing the initial damage, and it is shown that the higher the SHI irradiation temperature, the more efficient is the recovery process**.** Notably, the rate of recovery, defined as the relative magnitude of the decrease in disorder, significantly increases (by 25% in the less defective layers) when the irradiation temperature increases from 100 to 770 K. This higher efficiency at high temperature is attributed to the thermal load itself acting over longer timescale than the thermal spike associated with the energy deposition process of the SHIs. Cross sections in the range of a few square nanometers are determined, similar to those obtained for several other irradiation-induced defect-annealing experiments. The recovery cross section does not seem to depend on the temperature, except in the case of simultaneous low initial disorder and high irradiation temperature.

Merging all results allowed us to propose a two-step mechanism to explain the defect annealing observed upon ionizing conditions, irrespective of the irradiation characteristics and sequence. This mechanism is related to the partition into the SiC atomic and electronic subsystems and to the time and spatial dissipation scales of the deposited energy. These parameters, which depend on the disturbance of the crystalline network, directly govern the defect generation and annihilation rates that can also be affected by the macroscopic temperature. Therefore, we can conclude that an ionization-activated (first step), thermally assisted (second step) defect-annealing mechanism (referred to as the IATADA mechanism) occurs in SiC. This mechanism rationalizes the diverse descriptions reported so far in the literature.

The results presented in this paper bring information on the behavior of SiC in complex radiation environments and may be useful for both the qualification of this material for harsh conditions (e.g., in nuclear reactors) and the control of its disorder level (for instance, during or after ion beam doping). Finally, ionizing conditions as well as irradiation temperature are known to have a significant influence on defect accumulation rates in many materials, and the current work provides additional knowledge in the understanding of the various complex associated physical phenomena.

ACKNOWLEDGMENTS

Two of the authors (O.H.P. and W.J.W.) were supported by the U.S. Department of Energy, Office of Science, Basic Energy Sciences, Materials Sciences and Engineering Division, under Contract No. DE-AC05-00OR22725. The SHI irradiation experiments were performed at the Grand Accélérateur National d'Ions Lourds (GANIL), Caen, France, and the authors thank the CIRIL platform and the GANIL technical staffs. We acknowledge the French EMIR network for providing irradiation beam time. The TEM work carried out in Caen was partially supported by the ANR funding "Investissements d'Avenir" ANR-11-EQPX-0020, the FEDER, and by the Region Basse-Normandie.

[1] K. Nordlund, S. J. Zinkle, A. E. Sand, F. Granberg, R. S. Averback, R. Stoller, T. Suzudo, L. Malerba, F. Banhart, W. J. Weber, F. Willaime, S. L. Dudarev, and D. Simeone, Nat. Commun. **9**, 1084 (2018).

[2] A. E. Sand, R. Ullah, and A. A. Correa, npj Comput. Mater. **5**, 43 (2019).

[3] E. Wendler, A. Heft, and W. Wesch, Nucl. Instrum. Methods Phys. Res., Sect. B **141**, 105 (1998).

[4] J. Slotte, K. Saarinen, M. S. Janson, A. Hallén, A. Yu Kuznetsov, B. G. Svensson, J. Wong-Leung, and C. Jagadish, J. Appl. Phys. **97**, 033513 (2005).

[5] A. Debelle, L. Thomé, D. Dompoint, A. Boulle, F. Garrido, J. Jagielski, and D. Chaussende, J. Phys. D **43**, 455408 (2010).

[6] S. Sorieul, X. Kerbiriou, J.-M. Costantini, L. Gosmain, G. Calas, and Ch. Trautmann, J. Phys.: Condens. Matter. **24**, 201224 (2012).

[7] A. Debelle, M. Backman, L. Thomé, W. J. Weber, M. Toulemonde, S. Mylonas, A. Boulle, O. H. Pakarinen, N. Juslin, F. Djurabekova, K. Nordlund, F. Garrido, and D. Chaussende, Phys. Rev. B **86**, 100102(R) (2012).

[8] C. R. Eddy, Jr. and D. K. Gaskill, Science **324**, 1398 (2009).

[9] A. Morello, Nat. Mater. **14**, 135 (2015).

[10] J.-M. Lauenstein, M. Casey, A. Topper, E. Wilcox, A. Phan, S. Ikpe, and K LaBel, Poster Presentation at Institute of Electrical and Electronics Engineers (IEEE) Nuclear and Space Radiation Effects Conference (NSREC), Boston, MA,

July 16, 2015; https://ntrs.nasa.gov/archive/nasa/casi.ntrs.nasa.gov/20150020905.pdf.

[11] A. Benyagoub, A. Audren, L. Thomé, and F. Garrido, Appl. Phys. Lett. **89**, 241914 (2006).

[12] M. Backman, M. Toulemonde, O. H. Pakarinen, N. Juslin, F. Djurabekova, K. Nordlund, A. Debelle, and W. J. Weber, Comput. Mater. Sci. **67**, 261 (2013).

[13] Y. Zhang, R. Sachan, O. H. Pakarinen, M. F. Chisholm, P. Liu, H. Xue, and W. J. Weber, Nat. Commun. **6**, 8049 (2015).

[14] A. Debelle, M. Backman, L. Thomé, K. Nordlund, F. Djurabekova, W. J. Weber, I. Monnet, O. H. Pakarinen, F. Garrido, and F. Paumier, Nucl. Instrum. Methods Phys. Res., Sect. B **326**, 326 (2014).

[15] L. Thomé, G. Velisa, S. Miro, A. Debelle, F. Garrido, G. Sattonnay, S. Mylonas, P. Trocellier, and Y. Serruys, J. Appl. Phys. **117**, 105901 (2015).

[16] Y. Zhang, H. Xue, E. Zarkadoula, R. Sachan, Ch. Ostrouchov, P. Liu, X.-L. Wang, S. Zhang, T. S. Wang, and W. J. Weber, Curr. Opin. Sol. State Mater. Sci. **21**, 285 (2017).

[17] T. T. Hlatshwayo, J. H. O'Connell, V. A. Skuratov, E. Wendler, E. G. Njoroge, M. Mlambo, and J. B. Malherbe, RSC Adv. **6**, 68593 (2016).

[18] M. Ghaly, K. Nordlund, and R. S. Averback, Philos. Mag. A **79**, 795 (1999).

[19] F. Gao and W. J. Weber, Nucl. Instrum. Methods Phys. Res., Sect. B **191**, 504 (2002).

[20] M. Toulemonde, W. Assmann, C. Dufour, A. Meftah, F. Studer, and C. Trautmann, Mat. Fys. Medd. **52**, 263 (2006).

[21] D. Guo, I. Martin-Bragado, C. He, H. Zang, and P. Zhang, J. Appl. Phys. **116**, 204901 (2014).

[22] J. Wiktor, X. Kerbiriou, G. Jomard, S. Esnouf, M.-F. Barthe, and M. Bertolus, Phys. Rev. B. **89**, 155203 (2014).

[23] C.-O. Bacri, C. Bachelet, C. Baumier, J. Bourçois, L. Delbecq, D. Ledu, N. Pauwels, S. Picard, S. Renouf, and C. Tanguy, Nucl. Instrum. Methods Phys. Res., Sect. B **406**, 48 (2017).

[24] J. F. Ziegler, J. P. Biersack, and U. Littmark, *The Stopping and Range of Ions in Solids* (Pergamon, New York, 1985); Available at: www.srim.org.

[25] L. L. Snead, Y. Katoh, T. Koyanagi, K. Terrani, and E. D. Specht, J. Nucl. Mater. **471**, 92 (2016).

[26] L. Nowicki, A. Turos, R. Ratajczak, A. Stonert, and F. Garrido, Nucl. Instrum. Methods Phys. Res., Sect. B **240**, 277 (2005).

[27] M. Ishimaru, I.-T. Bae, A. Hirata, Y. Hirotsu, J. A.Valdez, and K. E. Sickafus, Nucl. Instrum. Methods Phys. Res., Sect. B **242**, 473 (2006).

[28] V. Heera, R. Kögler, W. Skorupa, and E. Glaser, MRS Proc. **316**, 229 (1993).

[29] K. Volz, J. K. N. Lindner, and B. Stritzker, Nucl. Instrum. Methods Phys. Res., Sect. B **120**, 133 (1996).

[30] A. Boulle, A. Debelle, J. B. Wallace, L. B. Bayu Aji, and S. O. Kucheyev, Acta Mater. **140**, 250 (2017).

[31] M.-J. Zheng, N. Swaminathan, D. Morgan, and I. Szlufarska, Phys. Rev. B **88**, 054105 (2013).

[32] W. J. Weber, W. Jiang, and S. Thevuthasan, Nucl. Instrum. Methods Phys. Res., Sect. B **166**, 410 (2000).

[33] H. Xue, Ph.D. Dissertation, University of Knoxville, 2015; https://trace.tennessee.edu/utk_graddiss/3486/.

[34] W. Jiang, H. J. Jung, L. Kovarik, Z. Wang, T. J. Roosendaal, Z. Zhu, D. J. Edwards, S. Hu, Ch. H. Henager, Jr., R. J. Kurtz, and Y. Wang, J. Nucl. Mater. **458**, 146 (2015).

[35] L. B. Bayu Aji, E. Stavrou, J. B. Wallace, A. Boulle, A. Debelle, and S. O. Kucheyev, Appl. Phys. A **125**, 28 (2019).

[36] Y. Adda, M. Beyeler, and G. Brebec, Thin Solid Films **25**, 107 (1975).

[37] H. Bernas, Amorphous systems and amorphization, in *Radiation Effects in Solids*, edited by K. E. Sickafus, E. A. Kotomin, and B. P. Uberuaga, NATO Science Series, Mathematics, Physics and Chemistry Vol. 235 (Elsevier, New York, 2004), Chap. 12.

[38] A. H. Mir, M. Toulemonde, C. Jegou, S. Miro, Y. Serruys, S. Bouffard, and S. Peuget, Sci. Rep. **6**, 30191 (2016).

[39] K. Jin, Y. Zhang, and W. J. Weber, Mater. Res. Lett. **6**, 531 (2018).

[40] M. Sall, I. Monnet, C. Grygiel, B. Ban d'Etat, H. Lebius, S. Leclerc, and E. Balanzat, Europhys. Lett. **102**, 26002 (2013).

[41] M. D. Mihai, P. Ionescu, D. Pantelica, H. Petrascu, D. Craciun, V. Craciun, F. Vasiliu, B. S. Vasile, and I. Mercioniu, Nucl. Instrum. Methods Phys. Res., Sect. B (2018), doi: 10.1016/j.nimb.2018.09.005.

[42] G. Gutierrez, D. Gosset, M. Bricout, C. Onofri, and A. Debelle, J. Nucl. Mater. **519**, 52 (2019).

[43] N. Sellami, A. Debelle, M. W. Ullah, H. M. Christen, J. K. Keum, H. Bei, H. Xue, W. J. Weber, and Y. Zhang, Curr. Opin. Solid State Mater. Sci. (2019), doi: 10.1016/j.cossms.2019.02.002.

[44] A. Debelle, J.-P. Crocombette, A. Boulle, E. Martinez, B. P. Uberuaga, D. Bachiller-Perea, Y. Haddad, F. Garrido, L. Thomé, and M. Béhar, Phys. Rev. Mater. **2**, 083605 (2018).

[45] P. Kalita, S. Ghosh, U. B. Singh, P. K. Kulriya, V. Grover, R. Shukla, A. K. Tyagi, G. Sattonnay, and D. K. Avasthi, J. Appl. Phys. **125**, 115902 (2019).